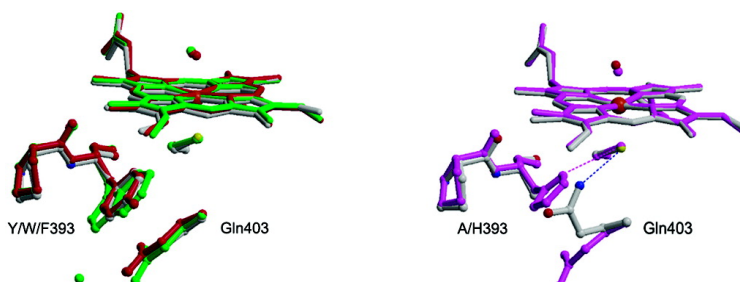Article

Oxygen Activation and Electron Transfer in Flavocytochrome P450 BM3

Tobias W. B. Ost, Jonathan Clark, Christopher G. Mowat, Caroline S. Miles,
Malcolm D. Walkinshaw, Graeme A. Reid, Stephen K. Chapman, and Simon Daff

More About This Article

Additional resources and features associated with this article are available within the HTML version:

- Supporting Information
- Access to high resolution figures
- Links to articles and content related to this article
- Copyright permission to reproduce figures and/or text from this article

View the Full Text HTML

Oxygen Activation and Electron Transfer in Flavocytochrome P450 BM3

Tobias W. B. Ost,*,† Jonathan Clark,† Christopher G. Mowat,†,‡ Caroline S. Miles,‡
Malcolm D. Walkinshaw,‡ Graeme A. Reid,‡ Stephen K. Chapman,† and
Simon Daff*,†

*Contribution from the School of Chemistry, University of Edinburgh, West Mains Road,
Edinburgh, EH9 3JJ, and The Institute of Cell and Molecular Biology, University of Edinburgh,
Mayfield Road, Edinburgh, EH9 3JT*

Received April 22, 2003; E-mail: Simon.Daff@ed.ac.uk

Abstract: In flavocytochrome P450 BM3, there is a conserved phenylalanine residue at position 393 (Phe393), close to Cys400, the thiolate ligand to the heme. Substitution of Phe393 by Ala, His, Tyr, and Trp has allowed us to modulate the reduction potential of the heme, while retaining the structural integrity of the enzyme's active site. Substrate binding triggers electron transfer in P450 BM3 by inducing a shift from a low- to high-spin ferric heme and a 140 mV increase in the heme reduction potential. Kinetic analysis of the mutants indicated that the spin-state shift alone accelerates the rate of heme reduction (the rate determining step for overall catalysis) by 200-fold and that the concomitant shift in reduction potential is only responsible for a modest 2-fold rate enhancement. The second step in the P450 catalytic cycle involves binding of dioxygen to the ferrous heme. The stabilities of the oxy-ferrous complexes in the mutant enzymes were also analyzed using stopped-flow kinetics. These were found to be surprisingly stable, decaying to superoxide and ferric heme at rates of $0.01-0.5$ s^{-1}. The stability of the oxy-ferrous complexes was greater for mutants with higher reduction potentials, which had lower catalytic turnover rates but faster heme reduction rates. The catalytic rate-determining step of these enzymes can no longer be the initial heme reduction event but is likely to be either reduction of the stabilized oxy-ferrous complex, i.e., the second flavin to heme electron transfer or a subsequent protonation event. Modulating the reduction potential of P450 BM3 appears to tune the two steps in opposite directions; the potential of the wild-type enzyme appears to be optimized to maximize the overall rate of turnover. The dependence of the visible absorption spectrum of the oxy-ferrous complex on the heme reduction potential is also discussed.

Introduction

Cytochromes P450 (P450s) are *b*-heme-containing monooxygenases implicated in numerous biosynthetic and metabolic processes.[1] They are able to catalyze oxygen atom insertion (eq 1) into a wide variety of substrates.

$$RH + O_2 + 2e^- \xrightarrow{\text{P450}} ROH + H_2O \qquad (1)$$

This is made possible by the ability of P450s to reductively activate molecular oxygen at the heme center. The heme-iron is axially ligated by a cysteine thiolate ligand; this distinguishes P450s from other oxygen activating enzymes such as the globins and peroxidases, which utilize histidine. The electronic influence of the axial ligand on the heme-iron in P450s is the key to their unique catalytic abilities.[2-5] The importance of cysteine as the

axial heme ligand can be inferred from its absolute conservation in every member of the P450 family and has been demonstrated to be essential for monooxygenase activity in studies of model complexes and mutant P450s.[6-9] The cysteine is believed to provide an electronic "push" to the heme-iron, which increases the electron density at the iron to promote the heterolytic cleavage of heme-bound dioxygen.[10,11]

Although the mechanism of oxygen activation by cytochromes P450 has been extensively studied,[12-15] the factors

† School of Chemistry.
‡ The Institute of Cell and Molecular Biology.
(1) Ortiz de Montellano, P. R., Ed. *Cytochrome P450: Structure, Mechanism and Biochemistry*, 2nd ed.; Plenum Press: New York, 1995.
(2) Dawson, J. H.; Holm, R. H.; Trundell, J. R.; Barth, G.; Linder, R. E.; Bunnenberg, E.; Djerassi, C.; Tang, S. C. *J. Am. Chem. Soc.* **1976**, *98*, 3707−3709.
(3) Poulos, T. L.; Finzel, B. C.; Gunsalus, I. C.; Wagner, G. C.; Kraut, J. *J. Biol. Chem.* **1985**, *260*, 16122−16130.
(4) Sono, M.; Roach, M. P.; Coulter, E. D.; Dawson, J. H. *Chem. Rev.* **1996**, *96*, 2841−2887.
(5) Ogliaro, F.; de Visser, S.; Shaik, S. *J. Inorg. Biochem.* **2002**, *91*, 554−567.
(6) Higuchi, T.; Uzu, S.; Hirobe, M. *J. Am. Chem. Soc.* **1990**, *112*, 7051−7053.
(7) Tani, F.; Matsu-ura, M.; Nakayama, S.; Nartua, Y. *Coord. Chem. Rev.* **2002**, *226*, 219−226.
(8) Auclair, K.; Moenne-Loccoz, P.; Ortiz de Montellano, P. R. *J. Am. Chem. Soc.* **2001**, *123*, 4877−4885.
(9) Vatsis, K.; Peng, H,-M.; Coon, M. J. *J. Inorg. Biochem.* **2002**, *91*, 542−553.
(10) Sono, M.; Dawson, J. H. *J. Biol. Chem.* **1982**, *257*, 5496−5502.
(11) Sono, M.; Andersson, L. A.; Dawson, J. H. *J. Biol. Chem.* **1982**, *257*, 8303−8320.
(12) Gerber, N. C.; Sligar, S. G. *J. Biol. Chem.* **1994**, *269*, 4260−4266.

controlling activation itself are less well understood. Dioxygen binds to ferrous heme-iron but has negligible affinity for the ferric form. Heme reduction occurs only after substrate binding, which induces a change in the iron coordination geometry from octahedral to square-based pyramidal, an event which is accompanied by a change from a low- to high-spin state at the ferric iron.[16,17] These steps initiate the P450 catalytic cycle, and their rigorously sequential nature helps to prevent unproductive cycling.[18] In a productive cycle, the oxy-ferrous complex (once formed) is reduced by a second electron from the reductase. On protonation, this complex decomposes to the reactive oxy-ferryl (Fe^{IV}=O) moiety responsible for oxygen atom insertion. Although this sequence of steps is common to all P450s, the rate at which the steps occur is highly variable as demonstrated by the variability in the catalytic turnover rates of the many P450 isoforms studied.[1] These are influenced by additional factors such as interprotein recognition, electron transfer, substrate recognition, and product release. Molecular oxygen activation must be carefully controlled in each case to ensure efficient substrate oxygenation without uncoupling, i.e., unproductive dissociation of reduced oxygen species from the heme prior to reaction with substrate.[18] P450s must therefore balance their ability to reduce molecular oxygen against their ability to stabilize reactive-oxygen intermediates. Other oxygen-binding hemoproteins have very different properties; oxidases promote the release of reduced oxygen species, while the globins reversibly bind dioxygen.[19-21] The question of how this balance is achieved is of fundamental importance.

While the sequence identity of P450s is quite low (typically 15-25%), particular regions do exhibit a high degree of identity. The heme binding loop runs from the heme ligand (Cys), through a glycine residue to a phenylalanine residue (Phe393 in P450 BM3), all of which are highly conserved.[22] This structural motif is fundamentally important to P450s since the Fe-Cys bond is the only formal bonding interaction between the heme and the protein. Substituting the cysteine ligand results in one of two outcomes, (i) catalytic deactivation or (ii) failure to incorporate heme,[8,9] both of which demonstrate the necessity for a cysteine ligand but neither of which explains why.

P450 BM3 is a single component fatty acid monooxygenase from *Bacillus megaterium*.[45] It is composed of a P450-heme-containing oxygenase domain, which is connected via a short protein linker to a diflavin reductase domain. The reductase domain is related to mammalian microsomal P450 reductase and binds 1 equiv each of FMN and FAD. The reductase domain functions as an NADPH dehydrogenase, supplying electron

equivalents directly to the heme. The unusual structure of P450 BM3 makes it an ideal model of a mammalian P450 system contained within a single component. It is particularly useful for studying how electron transfer is coupled to oxygen activation in the P450s. Our earlier studies showed how substitution of phenylalanine 393 of P450 BM3 influences the heme reduction potential and the stability of the oxy-ferrous complex.[23,24] Here, we extend this work to examine how the thermodynamic properties of the heme influence the key steps in the P450 catalytic cycle: electron transfer, and oxygen activation.

Experimental Procedures

***Escherichia coli* Strains and Plasmids.** The preparation of plasmids for the overexpression of full-length and heme domain constructs of WT P450 BM3 (pBM23 and pBM20), F3939A (pCM36 and pCM80), F393H (pCM37 and pCM81), and the F393Y (pCM109 and pCM125) mutant enzymes has been reported previously.[23] The F393W mutant was constructed by oligonucleotide-directed mutagenesis of the wild-type plasmids pJM23 and pJM20, respectively, using the Kunkel method.[25] The oligonucleotide primer used in the mutagenesis procedure is shown below (mismatches are indicated by the italicized bases) 5′CTGACCGTTTCC*CC*ACGGTTTAAACG 3′. The resulting full-length and heme domain constructs were named pCM111 and pCM110, respectively. Both plasmids were sequenced on a Perkin-Elmer ABI Prism 377 DNA sequencer to ensure no secondary mutations had occurred. The *E. coli* strain TG1 [*sup*E, *hsd*Δ5, *thi*, Δ(*lac-pro*AB), F′ [*tra*Δ36, *pro*AB+, *lac*I�q, *lac*ZΔM15]] was used for all cloning work and for overexpression of the full-length and heme domain proteins.

Enzyme Preparations. All enzymes were isolated and purified as described previously.[23] All pure proteins were concentrated to >500 μM by ultrafiltration and were flash frozen in liquid nitrogen prior to storage at −80 °C. Enzymes were used within 1 month of isolation.

Spectrophotometric Analysis of Fatty Acid and Carbon Monoxide Binding to P450s. UV/visible absorption spectra were recorded over the 300−800 nm range using a Shimadzu 2101 spectrophotometer and quartz cuvettes of 1 cm path length. Typically, the concentration of P450 BM3 used was 1−5 μM in 1 mL of assay buffer (100 mM MOPS pH 7.0) at 30 °C. Substrate dissociation constants were determined for arachidonate and laurate according to established procedures.[23]

Steady-State Kinetics. All steady-state kinetic measurements were performed at 15 °C in air saturated assay buffer using 1 cm path length quartz cuvettes. Initial rates of NADPH oxidation were measured, as described previously,[23] by monitoring the decrease in absorbance of NADPH (ϵ_{340} = 6.21 mM^{-1} cm^{-1}) with time, under substrate-free or substrate-saturating ([arachidonate] = 100 μM) conditions. Enzyme concentrations used were typically 2−10 μM for substrate-free assays and 10−100 nM for arachidonate-saturated assays. The quoted rate constants (k_{cat}) are the average of three separate experiments.

Pre-Steady-State Kinetics. All pre-steady-state measurements were performed at 15 °C using an Applied Photophysics stopped-flow spectrophotometer (SX.17MV) contained within an anaerobic glovebox (Belle Technology; [O$_2$] < 5 ppm) using either single-wavelength or diode-array detectors.

A. Heme Reduction. Rate constants for the first flavin-to-heme electron-transfer step (k_{red}) were determined by monitoring the formation of the ferrous-CO (Fe^{II}−CO) adduct of the full-length flavocytochromes with time. One syringe contained NADPH (100 μM), and the second

(13) Benson, D. E.; Suslick, K. S.; Sligar, S. G. *Biochemistry* **1997**, *36*, 5104−5107.
(14) Schlichting, I.; Berendzen, J.; Chu, K.; Stock, A. M.; Maves, S. A.; Benson, D. E.; Sweet, R. M.; Ringe, D.; Petsko, G. A.; Sligar, S. G. *Science* **2000**, *287*, 1615−1622.
(15) Davydov, R.; Makris, T. M.; Kofman, V.; Werst, D. E.; Sligar, S. G.; Hoffman, B. M. *J. Am. Chem. Soc.* **2001**, *123*, 1403−1415.
(16) Sligar, S. G. *Biochemistry* **1976**, *15*, 5399−5406.
(17) Tsai, R.; Yu, C. A.; Gunsalus, I. C.; Peisach, J.; Blumberg, W.; Orme-Johnson, W. H.; Beinert, H. *Proc. Natl. Acad. Sci. U.S.A.* **1970**, *66*, 1157−1163.
(18) Loida, P. J.; Sligar, S. G. *Biochemistry* **1993**, *32*, 11530−11538.
(19) Jones, R. D.; Summerville, D. A.; Basolo, F. *Chem. Rev.* **1979**, *79*, 139−179.
(20) Chapman, S. K.; Daff, S.; Munro, A. W. *Struct. Bonding* **1997**, *88*, 39−70.
(21) Dawson, J. H. *Science* **1988**, *240*, 433−439.
(22) Nelson, D. R.; Koymans, L.; Kamataki, T.; Stegeman, J. J.; Feyereisen, R.; Waxman, D. J.; Waterman, M. R.; Gotoh, O.; Coon, M. J.; Estabrook, R. W.; Gunsalus, I. C.; Nerbert, D. W. *Pharmacogenetics* **1996**, *6*, 1−42.
(23) Ost, T. W. B.; Miles, C. S.; Munro, A. W.; Murdoch, J.; Reid, G. A.; Chapman, S. K. *Biochemistry* **2001**, *40*, 13421−13429.
(24) Ost, T. W. B.; Munro, A. W.; Mowat, C. G.; Taylor, P. R.; Pesseguiero, A.; Fulco, A. J.; Cho, A. K.; Cheesman, M. R.; Walkinshaw, M. D.; Chapman, S. K. *Biochemistry* **2001**, *40*, 13430−13438.
(25) Kunkel, W. H. *Proc. Natl. Acad. Sci. U.S.A.* **1985**, *82*, 488−492.

Table 1. Thermodynamic and Kinetic Parameters Determined for Wild-Type and the F393 Series of Mutant Enzymes of Flavocytochrome P450 BM3[g]

	enzyme				
	F393A	F393H	F393Y	WT	F393W
Substrate-bound (SB)[a]					
reduction potential (mV)[c,d]	-151 ± 4	-176 ± 4	-295 ± 6	-289 ± 5	-360 ± 5
turnover (k_{cat}, s^{-1})[e]	18 ± 2	21 ± 2	66 ± 7	67 ± 7	41 ± 4
heme reduction (k_{red}, s^{-1})[e]	240 ± 24	205 ± 21	94 ± 10	99 ± 10	29 ± 3
autoxidation (k_{autox}, $\times 10^3$ s^{-1})[e]	10 ± 1	3 ± 1	110 ± 10	140 ± 10	540 ± 50
Substrate-free (SF)[b]					
reduction potential (mV)[c,d]	-312 ± 4	-332 ± 6	-418 ± 6	-427 ± 4	-480 ± 5
turnover (k_{cat}, s^{-1})[e]	0.27 ± 0.03	0.28 ± 0.03	0.12 ± 0.01	0.09 ± 0.01	0.08 ± 0.01
heme reduction					
slow phase (k_{reds}, s^{-1})[e,f]	0.3 ± 0.1 (71%)	0.2 ± 0.1 (48%)	0.2 ± 0.1 (18%)	0.14 ± 0.05 (28%)	0.3 ± 0.1 (11%)
fast phase (k_{redf}, s^{-1})[e,f]	3.1 (24%)	1.3 (14%)	0.9 (6%)	2.6 (8%)	11 (15%)
autoxidation (k_{autox}, $\times 10^3$ s^{-1})[e]	10 ± 1	5 ± 1	90 ± 9	110 ± 20	440 ± 50

[a] Determined in the presence of saturating concentrations (100 μM) arachidonate. [b] Determined in the absence of substrate. [c] Values for wild-type, F393A, F393H, and F393Y reported in ref 23. [d] Experiments conducted at 25 °C in 100 mM KPi pH 7.0 except for F393W where the buffer was 100 mM Tris/500 mM KCl, pH 7.0. [e] Experiments conducted at 15 °C in 100 mM MOPS pH 7.0. [f] Heme reduction slow phase (k_{reds}) and fast phase (k_{redf}), with percentage of total heme reduction in each phase. [g] Experimental conditions are described in the Experimental Procedures section.

syringe contained full-length wild-type or mutant P450 BM3 (1–5 μM). Both syringes contained anaerobic assay buffer previously saturated with CO by bubbling for 5 min ([CO] = $\sim$200μM). In the case of the substrate-saturated experiments, full conversion (>95%) to the Fe^{II}–CO complex was observed; the data were monophasic and were evaluated by fitting the absorbance change to a single-exponential function (λ_{obs} = 450 nm (WT, F393Y, F393W), 445 nm (F393H), and 444 nm (F393A)). In the absence of substrate, incomplete conversion to the Fe^{II}–CO complex was observed; the data were biphasic and were evaluated by fitting the absorbance change to a double exponential function. The slow phase constituted the greatest proportion of the amplitude. Analyses were performed using Microcal Origin 7 software. Values quoted are from the averages of four separate measurements. Rate constants determined for the fast phase were less predictable; examples are shown in Table 1.

B. Autoxidation. Rate constants (k_{autox}) for the decay of the oxy-ferrous complexes of the wild-type and mutant P450 BM3 heme domains were determined by monitoring the rates of autoxidation to ferric P450 with time. The heme domain proteins ($\sim$10 μM) were prereduced by addition of 40 μM sodium dithionite. Excess dithionite was removed prior to experimentation by elution of the reduced P450s through a pre-equilibrated 10 mL G25 gel-filtration column. Reduction was confirmed by UV/visible spectrometry on a Varian Cary 50 Bio spectrophotometer, also contained within the glovebox. Formation of the oxy-ferrous complex was achieved by mixing the reduced P450 (syringe A) with air-saturated assay buffer ([O$_2$] $\approx$ 200 μM (syringe B)). Formation of the oxy-ferrous species was too fast to measure (>600 s^{-1}), yet in each case, the decay occurred over a period of seconds and could be conveniently measured. Autoxidation of ferrous P450 (Fe^{2+} – O$_2$ → Fe^{3+} + O$_2^-$) was followed using a PDA detector across the range 300–700 nm. The variation in A$_{470}$ with time was monophasic for both the substrate-free and substrate-saturated experiments and was evaluated by fitting the data to a single exponential (Microcal Origin 7). This wavelength gave the most consistent results over all the different conditions. For substrate-free enzyme some high to low spin conversion can be seen in the Soret region over long time scales. Over short time scales, some oxyferrous formation can also be observed.

Optically Transparent Thin Layer Electrochemical (OTTLE) Potentiometry. Spectroelectrochemical analysis of the F393W mutant heme domain was conducted in an OTTLE cell constructed from a modified quartz EPR cell with a 0.3 mm path length, containing a Pt/Rh (95/5) gauze working electrode (wire diameter 0.06 mm, mesh size 1024 cm^{-1}, Engelhardt, UK), a platinum wire counter electrode and a Ag/AgCl reference electrode (model MF2052, Bioanalytical Systems, IN 47906, USA). Enzyme samples (0.5 mL $\times$ 100–200 μM) were eluted through a G25 column pre-equilibrated with 0.1 M Tris pH 7.5,

0.5 M KCl in an anaerobic glovebox. The following mediators were then added: 2-hydroxy-1,4-naphthoquinone (20 μM), FMN (5 μM), benzyl viologen (10 μM) and methyl viologen (10 μM). Spectroelectrochemical titrations were performed at 25 $\pm$ 2 °C using an Autolab PGSTAT10 potentiostat and a Cary 50 UV/vis spectrophotometer. The potential of the working electrode was decreased in 30 mV steps until the enzyme was fully reduced and increased stepwise until reoxidation was complete. After each step, the current and UV/vis absorption spectrum were monitored until no further change occurred. This equilibration process typically lasted 15 min. Absorbance changes were plotted against the potential of the working electrode and analyzed using the Nernst equation. The Ag/AgCl reference electrode employed in the OTTLE cell was calibrated against indigotrisulfonic acid (E_m = -99 mV vs SHE) and FMN (E_m = -220 mV vs SHE) in the same buffer conditions. All electrode potentials were corrected accordingly by $+182$ $\pm$ 2 mV relative to the standard hydrogen electrode.

Crystallization and Refinement. Crystallizations of F393A, -W, and -Y heme domains were carried out by hanging drop vapor diffusion at 4 °C in Linbro plates. Crystals were obtained with a well solution comprising 100 mM sodium PIPES, pH 6.5–7.5, 40 mM MgSO$_4$, and 18–21% PEG 8000. Hanging drops of 4 μL were prepared by adding 2 μL of 40 mg/mL protein (in 50 mM TrisHCl/1 mM EDTA, pH 7.4) to 2 μL of well solution. Plates of up to 1 $\times$ 0.3 $\times$ 0.3 mm^3 were formed after about 1 week. Crystals were immersed in well solution containing 22% glycerol as a cryoprotectant, prior to mounting in nylon loops and flash-cooling in liquid nitrogen. For the F393A mutant heme domain, a data set was collected to a 2.05 Å resolution on beamline $\times$11 (λ = 0.8482 Å) at DESY Hamburg, for the F393W heme domain, a data set was collected to a 2.0 Å resolution on beamline BM14 (λ = 1.0332 Å) at ESRF Grenoble, and for the F393Y heme domain, a data set was collected to a 2.0 Å resolution on beamline $\times$13 (λ = 0.802 Å) at DESY Hamburg. All data were collected using a Mar CCD detector. Crystals of all three mutant forms belong to space group $P2_1$. Crystals of the F393A heme domain were found to have the following cell dimensions: a = 58.694 Å, b = 152.911 Å, c = 61.197 Å, and β = 94.640°. Those of the F393W heme domain had the following dimensions: a = 58.911 Å, b = 153.538 Å, c = 61.430 Å, and β = 94.424°. Those of the F393Y heme domain had the following dimensions: a = 59.608 Å, b = 152.983 Å, c = 61.774 Å, and β = 94.539°. Data processing was carried out using the HKL package.[26] The wild-type flavocytochrome P450 BM3 heme domain structure (2HPD),[27] stripped of water, was used as the initial model. Electron

(26) Otwinowski, Z.; Minor, W. *Methods Enzymol.* **1997**, *276*, 307–326.
(27) Ravichandran, K. G.; Boddupalli, S. S.; Hasemann, C. A.; Peterson, J. A.; Deisenhofer, J. *Science* **1993**, *261*, 731–736.

density fitting was carried out using the program TURBO-FRODO[28] (in *Silicon Graphics Geometry Partners Directory 86*, Silicon Graphics, Mountain View, CA). Structure refinement was carried out using Refmac.[29] The atomic coordinates have been deposited in the Protein Data Bank (1P0V:F393A; 1P0W:F393W; 1P0X:F393Y).

Results

Characterization of the F393W Mutant. The ferrous F393W mutant (in both full-length and heme domain) formed a typical P450 complex with CO, with a Soret absorption maximum at 449 nm. Titration of the mutant enzyme with substrate (either arachidonate or laurate) induced a shift in the absorption spectrum consistent with the low- to high-spin transition of ferric heme iron. The substrate dissociation constants were determined to be 578 ± 35 μM for laurate and 2.0 ± 0.4 μM for arachidonate, both of which are similar to values determined for the wild-type enzyme. The most obvious change caused by the mutation is a large decrease in the heme reduction potential in the presence and absence of substrate. These values are -480 ± 5 mV and -360 ± 5 mV for the substrate-free and substrate-saturated F393W heme domain, respectively (Table 1), compared to values of -427 mV and -289 mV for the wild-type enzyme, respectively. These potentials are substantially more negative than the midpoint potential of NADPH (-320 mV) and probably also of the FMN cofactor of P450 BM3,[48] making electron transfer to the heme in the F393W mutant enzyme thermodynamically unfavorable even in the presence of substrate. In the wild-type enzyme, heme reduction in the presence of NADPH is favored only after substrate binding. This effect, together with the spin-state change, acts as an electron-transfer control mechanism. The other mutants included in this study have been characterized previously:[23,24] the F393A and F393H mutants both have higher reduction potentials than the wild-type enzyme and blue-shifted Soret absorption bands for their ferrous heme-CO complexes. The F393Y mutant, on the other hand, is similar to the wild-type enzyme in these respects. All the mutants have similar substrate binding affinities and associated spin-state shifts. This is the first indication that some key properties of the enzyme active site are unaffected by the mutation despite the large shifts either way in heme reduction potential.

Steady-State Kinetics. The k_{cat} values for wild-type P450 BM3 and the F393A, -H, -Y, and -W mutants are shown in Table 1. The background rate constant for NADPH oxidation in the absence of substrate is small ($k_{cat} < 0.3$ s^{-1}) for all the mutants, and in all cases, the k_{cat} increases by 2 orders of magnitude ($18-67$ s^{-1}) in the presence of substrate. This is consistent with the established idea that substrate binding gates electron transfer to the heme, such that reducing equivalents are only consumed when substrate is present. The F393W mutant was found to couple NADPH consumption to substrate monooxygenation with greater than 90 % efficiency. The other mutants and the wild-type enzyme couple similarly well[23] (i.e. >80%) except for the F393A mutant, which is slightly less efficient (56% coupling). The substrate saturated k_{cat} varies across the series of enzymes studied (WT $\approx$ F393Y > F393W $\gg$ F393H $\approx$ F393A) by approximately 3-fold, but there is no

(28) Roussel, A.; Cambillau, C. *Silicon Graphics Geometry Partners Dictionary 86*; Silicon Graphics: Mountain View, CA.
(29) Murshudov, G. N.; Vagin, A. A.; Dodson, E. J. *Acta Crystallogr.* **1997**, *D53*, 240−255.
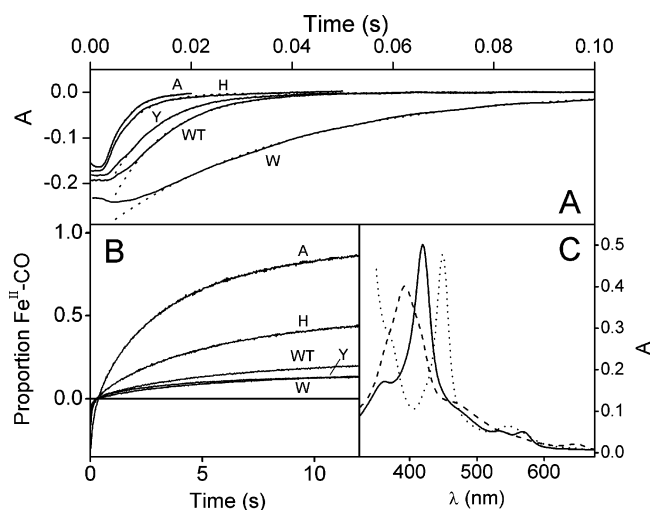
Figure 1. Heme reduction of flavocytochrome P450 BM3. Panels A and B show the time courses for formation of the P450 complex from the substrate-saturated (A) and substrate-free (B) forms of the wild-type (WT) and mutant enzymes. Each trace is labeled with the one letter code corresponding to the particular F393X substitution and is shown fitted to a single (panel A) or double (panel B) exponential function. The abscissa in panel B has been rescaled to show the proportion of ferrous CO complex formed during the second (slow) exponential phase (k_{reds}). For wavelengths, see Experimental Procedures. Panel C shows the absorption spectra of substrate-free ferric (solid line), substrate-bound ferric (broken line), and the ferrous-CO complex (dotted line) of the wild-type enzyme.

linear correlation with reduction potential. The wild-type enzyme has the largest k_{cat} (67 s^{-1}), and this is similar to the F393Y mutant (which has a similar reduction potential). The F393W mutant turns over at half this rate and has a more negative reduction potential. The F393H and F393A mutants on the other hand are slower still but have more positive reduction potentials. This complex trend suggests that the reduction potential of the wild-type enzyme is optimized to give the fastest overall catalytic rates.

Heme Reduction. In a series of stopped-flow experiments, rate constants were determined for the formation of ferrous CO complex on reaction of the holoenzymes with NADPH (Figure 1). These data (Table 1) approximate to the rate of first electron transfer to the heme. The ferrous form generated by electron transfer to the heme, is trapped by CO binding.[49] Binding of CO by reduced enzyme is rapid, occurring at rates in excess of 1000 s^{-1} in CO-saturated buffer in the wild-type and mutant enzymes. The overall process has many individual steps, most of which occur quickly, nevertheless, slight lag phases can be observed in some of the traces in Figure 1. A contributing factor may be reduction of the flavins, which is also a multiphasic process observed at 450 nm as a decrease in absorbance.[49] In the absence of substrate the heme reduction traces are biphasic, with a small fast phase being followed by a larger slow phase. The fast phase showed no obvious trend and varies erratically (examples only are presented in Table 1). Larger fast phases are obtained with enzyme containing a larger proportion of high-spin heme this has been found to result from contamination with detergents during preparation, which bind irreversibly to the enzyme. The slow phase was consistent for all the mutants, with very little change across the series. However, its amplitude appears to increase with reduction potential. It appears that the electron-transfer process is an equilibrium, the position of which depends on the reduction potential of the CO-bound heme and

Scheme 1
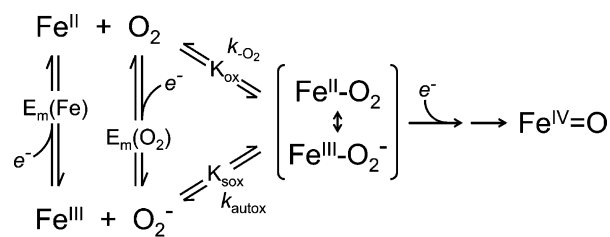
E_m (Fe) = Substrate bound heme reduction potential;
E_m (O_2) = One electron reduction potential of dioxygen;
K_{ox} = Equilibrium constant for oxygen binding;
K_{sox} = Equilibrium constant for superoxide binding;
k_{-O_2} = Rate constant for oxygen dissociation;
k_{autox} = Rate constant for superoxide dissociation;
e^- = electron.

Figure 2. Formation and decay of the oxy-ferrous species of the P450 BM3 F393A-heme domain at 15 °C under substrate-free (panel A) and substrate-saturating conditions (panel B). In both cases, the oxy-ferrous species is shown by the broken line, the solid lines correspond to ferric low-spin (panel A) and high-spin P450 (panel B). Panel C shows the exponential decay (k_{autox}) of substrate-free (upper trace) and substrate-saturated (lower trace) oxy-ferrous complexes, monitored at 470 nm. Both are shown fitted to single-exponential decay functions.

that of the FMN. The rate constants observed are then the sum of the forward and reverse rate constants. With this taken into account, in the absence of substrate, heme reduction appears to be slow enough to limit steady-state turnover for all the enzymes studied ($k_{reds}^{SF} < 0.4$ s^{-1}). For the F393W mutant, the rate constant (slow phase) determined for heme reduction is 5-fold faster than k_{cat}, but only 11% heme reduction occurs in the slow phase, suggesting that the reverse process is favored by the extremely negative heme reduction potential.

In the presence of substrate, the rate constants for heme reduction increase by 2 orders of magnitude (k_{red} is 29 s^{-1} or more) for all the enzymes studied. However, there is now a clear correlation with the heme reduction potential. At more negative reduction potentials (i.e., for the F393W and F393Y mutants and the wild-type enzyme) the rate of heme reduction slows and is similar to the rate of catalytic turnover, indicating that FMN to heme electron transfer is rate determining. At more positive reduction potentials, the rate of heme reduction is faster: k_{red} for the F393A mutant in the presence of substrate is 10-fold greater than for the F393W mutant. However, the rate of catalytic turnover is slower, such that k_{red} is now 10-fold greater than k_{cat}. This indicates that a change in the rate-determining step has occurred for the F393A and F393H mutants.

Oxy-Ferrous Decay. In the P450 catalytic cycle, heme reduction is followed by the binding of dioxygen, to form an oxy-ferrous/superoxy-ferric complex (Scheme 1). This is the starting point for the multistep oxygen activation process. Using rapid-scanning UV/vis stopped-flow spectrophotometry we were able to obtain spectra of the oxy-ferrous complexes of all the mutants and the wild-type enzyme and monitor their rates of decay to ferric heme, probably via the dissociation of superoxide. Figures 2−4 show the spectra of the wild-type enzyme and the F393A and F393W mutants in the presence and absence of substrate, and their respective time-courses for decay. The Soret peak positions were at 423 and 425 nm for the substrate-free and substrate-bound oxy-ferrous complexes respectively, regardless of mutation, but differences were observed in the long-wavelength region. These are shown in Figure 5, panel C. The similarities of the Soret bands of the mutant enzymes spectra indicate that they are all of oxy-ferrous complexes. The differences observed in the α−β region are not, therefore, due to contamination by oxidation products, but indicate that the heme electronic structure is perturbed by the mutations.

Although decay of the oxy-ferrous complex is a nonproductive process so far as catalytic turnover is concerned, its rate is
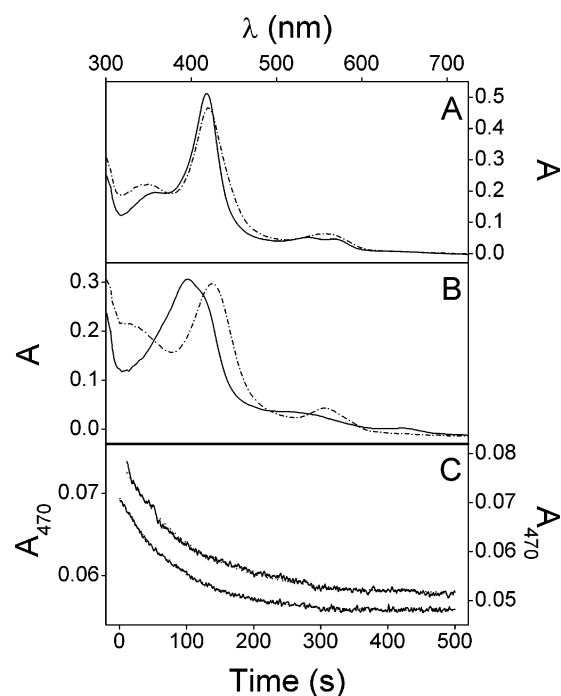
indicative of complex stability. The oxy-ferrous complexes of all the F393X enzymes decayed to the ferric high-spin form in the presence of substrate and primarily to low-spin ferric heme in the absence of substrate, as expected. However, in the latter reaction, a proportion of the enzyme remained high-spin (<20%), possibly due to oxidative damage of the active site. Rate constants for the autoxidation of the ferrous P450s in the absence (k_{autox}^{SF}) and presence of substrate (k_{autox}^{SB}) are shown in Table 1. Two major observations can be made. First, the autoxidation rate is essentially independent of the presence of substrate. This indicates that substrate has little effect on the stability of the oxy-ferrous complex in this P450 and is unlikely to be involved directly in catalytic oxygen activation. The slight increase in stability may be a reflection of the increased hydrophobicity of the active site when substrate is bound.

Second, the oxy-ferrous decay rate constants correlate with the heme reduction potentials. The F393H oxy-ferrous complex was the most long-lived ($k_{autox}^{SB} = 3.0 \times 10^{-3}$ s^{-1}), with a 40-fold slower autoxidation rate than the oxy-ferrous complex of the wild-type enzyme ($k_{autox}^{SB} = 0.14$ s^{-1}). The F393W oxy-ferrous complex, on the other hand, decayed 4 times faster ($k_{autox}^{SB} = 0.54$ s^{-1}) than that of the wild-type enzyme. The oxy-ferrous complex is therefore destabilized in mutants with lower reduction potentials and *vice versa*. The formation of superoxide on decay of the oxy-ferrous complex is likely to contribute to uncoupled turnover of the enzymes. The viability of this can be ascertained by comparing the rate constants for oxy-ferrous decay to the steady-state turnover rates. In the presence of substrate, catalytic turnover is 2 orders of magnitude faster than autoxidation for all the mutants, indicating that uncoupling via this route is not viable. Coupling percentages
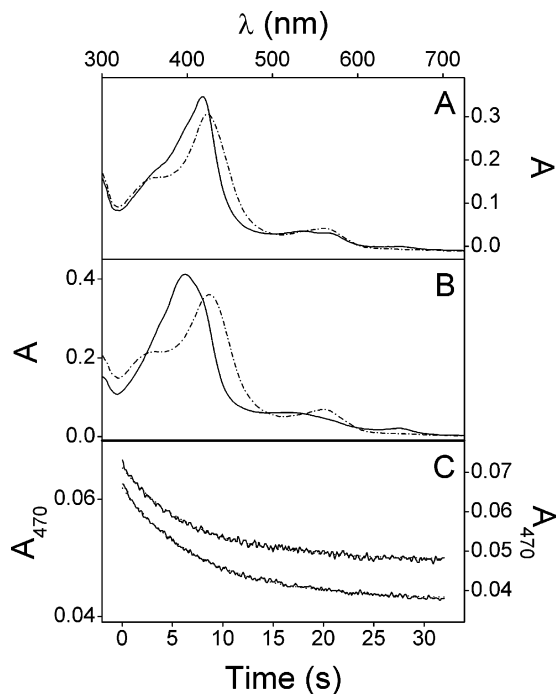
Figure 3. Formation and decay of the oxy-ferrous species of the wild-type P450 BM3 heme domain at 15 °C under substrate-free (panel A) and substrate-saturating conditions (panel B). In both cases, the oxy-ferrous species is shown by the broken line, the solid lines correspond to ferric low-spin (panel A) and high-spin P450 (panel B). Panel C shows the exponential decay (k_{autox}) of substrate-free (upper trace) and substrate-saturated (lower trace) oxy-ferrous complexes, monitored at 470 nm. Both are shown fitted to single-exponential decay functions.

Figure 4. Formation and decay of the oxy-ferrous species of the P450 BM3 F393W-heme domain at 15 °C under substrate-free (panel A) and substrate-saturating conditions (panel B). In both cases, the oxy-ferrous species is shown by the broken line, the solid lines correspond to ferric low-spin (panel A) and high-spin P450 (panel B). Panel C shows the exponential decay (k_{autox}) of substrate-free (upper trace) and substrate-saturated (lower trace) oxy-ferrous complexes, monitored at 470 nm. Both are shown fitted to single-exponential decay functions.

were found to be greater than 90% for all mutants except the F393A mutant (56%), which must uncouple after the second electron transfer event. In the absence of substrate, the rate of background turnover appears to be limited by the rate of heme reduction, however, subsequent electron transfer events are likely to be faster than autoxidation avoiding the generation of superoxide. For the F393A and F393H mutants substrate-free turnover is > 30-fold faster than autoxidation, indicating that this is the case.

Crystal Structures. Data sets to a resolution of 2.0 Å (2.05 Å for F393A) were used to refine the structures of the F393A, F393W, and F393Y heme domains to final R-factors of 16.87% ($R_{free} = 23.73\%$), 15.93% ($R_{free} = 22.13\%$), and 17.17% ($R_{free} = 23.70\%$) respectively (Table 2). For the F393A-heme domain, the final model consists of two protein molecules (molecule A comprising residues Lys3-Leu188 and Asn201-Leu455; molecule B comprising Lys3-Leu188 and Tyr198-Leu455) each containing 1 heme and a total of 1408 water molecules. For the F393W-heme domain and F393Y-heme domain, each of the final models consists of two protein molecules (molecule A comprising residues Lys3-Leu188 and Asn201-Leu455; molecule B comprising Lys3-Arg190 and Pro196-Leu455) each containing 1 heme and a total of 1420 and 1238 water molecules, respectively. For all molecules, the electron density for the first two N-terminal residues and all (or most of) the loop region containing residues Gln189-Glu200 was uninterpretable, so these have been omitted from the model. The RMSD fit of all backbone atoms for each of the F393X-heme domain structures and the wild-type heme domain is 0.3 Å indicating no major differences between the four structures. Due to the presence of two molecules in the asymmetric unit for each of these models,
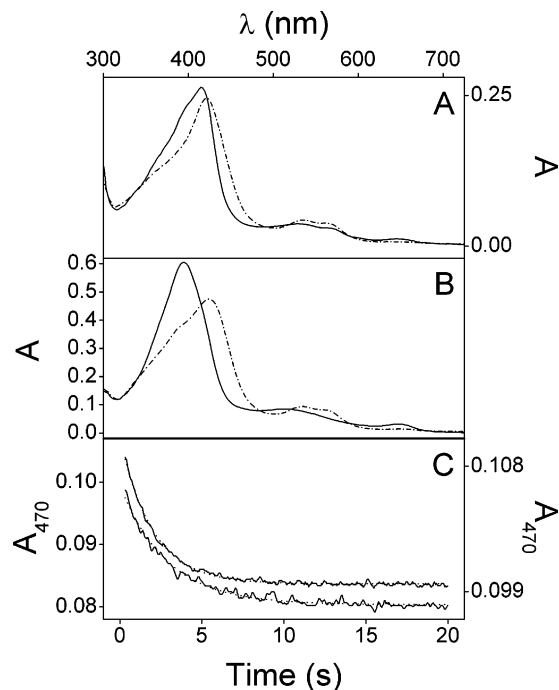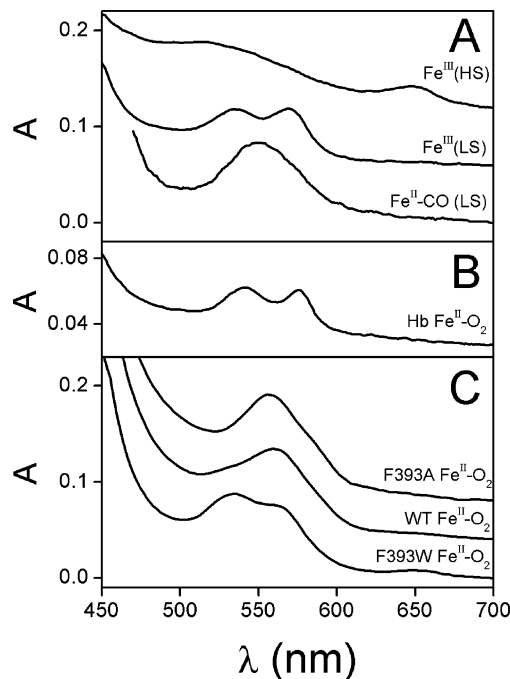

Figure 5. Comparison of the visible absorption spectra of P450 BM3 with oxyhemoglobin. Panel A shows the characteristic visible absorption spectra of the ferric high-spin (Fe^{III} (HS)), ferric low-spin (Fe^{III} (LS)) and carbonmonoxy-ferrous ($Fe^{II}-CO$ (LS)) forms of the wild-type P450 BM3 heme domain. Panel B shows the visible absorption spectrum of oxy-hemoglobin ($Fe^{II}-O_2$). Panel C shows the visible absorption spectra of the oxy-ferrous complexes ($Fe^{II}-O_2$) of F393A, wild-type, and F393W P450 BM3 heme domains.

the RMSD values stated are the average over both molecules. In addition, the RMSD fit between both molecules (A and B)

Table 2. Data Collection and Refinement Statistics

	F393A	F393W	F393Y
resolution (Å)	20.0−2.05	20.0−2.0	17.0−2.0
total no. of reflections	361 447	498 626	837 703
no. of unique reflections	66 956	72 855	67 437
completeness (%)	98.7	99.6	91.0
$(I)/[\sigma(I)]$	8.6	13.2	10.0
$R_{merge}{}^a$ (%)	8.6	6.5	8.5
R_{merge} in outer shell (%)	24.5	20.9	18.3
	(2.12−2.05 Å)	(2.12−2.0 Å)	(2.07−2.0 Å)
$R_{cryst}{}^b$ (%)	16.87	15.93	17.17
$R_{free}{}^b$ (%)	23.73	22.13	23.70
RMSD from ideal values:			
bond lengths (Å)	0.013	0.012	0.013
bond angles (deg)	2.8	2.4	2.6
ramachandran analysis:			
most favored (%)	90.9	90.7	91.4
additionally allowed (%)	8.6	8.8	8.1

^{a} $R_{merge} = \Sigma_h\Sigma_i|I(h) - I_I(h)|/\Sigma_h\Sigma_iI_I(h)$, where $I_I(h)$ and $I(h)$ are the ith and mean measurement of reflection h, respectively. ^{b} $R_{cryst} = \Sigma_h|F_o - F_c|/\Sigma_h F_o$, where F_o and F_c are the observed and calculated structure factor amplitudes of reflection h, respectively. R_{free} is the test reflection data set, 5% selected randomly for cross validation during crystallographic refinement.

is ∼0.2 Å for each of the mutant enzyme structures. Electron density for the heme binding region of each of the F393X-heme domain structures is shown in Figure 6. Apart from the expected structural difference associated with the change in the side chain caused by the substitution of phenylalanine 393, the heme binding region of all of these mutant forms remains relatively unperturbed by the particular substitution. The exception to this is the F393A mutant where a conformational change in the orientation of a nearby surface glutamine residue (Gln403) occurs. Comparison of the WT and the other mutant structures shows that the amide side chain of Gln403 points away from the heme, out toward the protein:solvent interface. However, in the case of the F393A-heme domain mutant structure, this glutamine has flipped ∼ 45° toward the heme, with the amide head occupying the void left by the substitution of the bulky phenyl side chain of F393 by alanine (Figure 7a). The amide group of Gln403 is the same distance (3.6 Å) from the heme ligand as the histidine side chain is in the F393H mutant (3.7 Å). Both may form hydrogen-bonding interactions with Cys400. This would explain why the redox properties of the two mutant enzymes are so similar; they are the result of a common interaction. A hydrogen bond to the axially ligating cysteine would be expected to reduce its potency as a strong σ and π donor, leading to the increase in heme reduction potential observed. The imidazole group of the F393H mutant may also mediate the reduction potential by electrostatically interacting
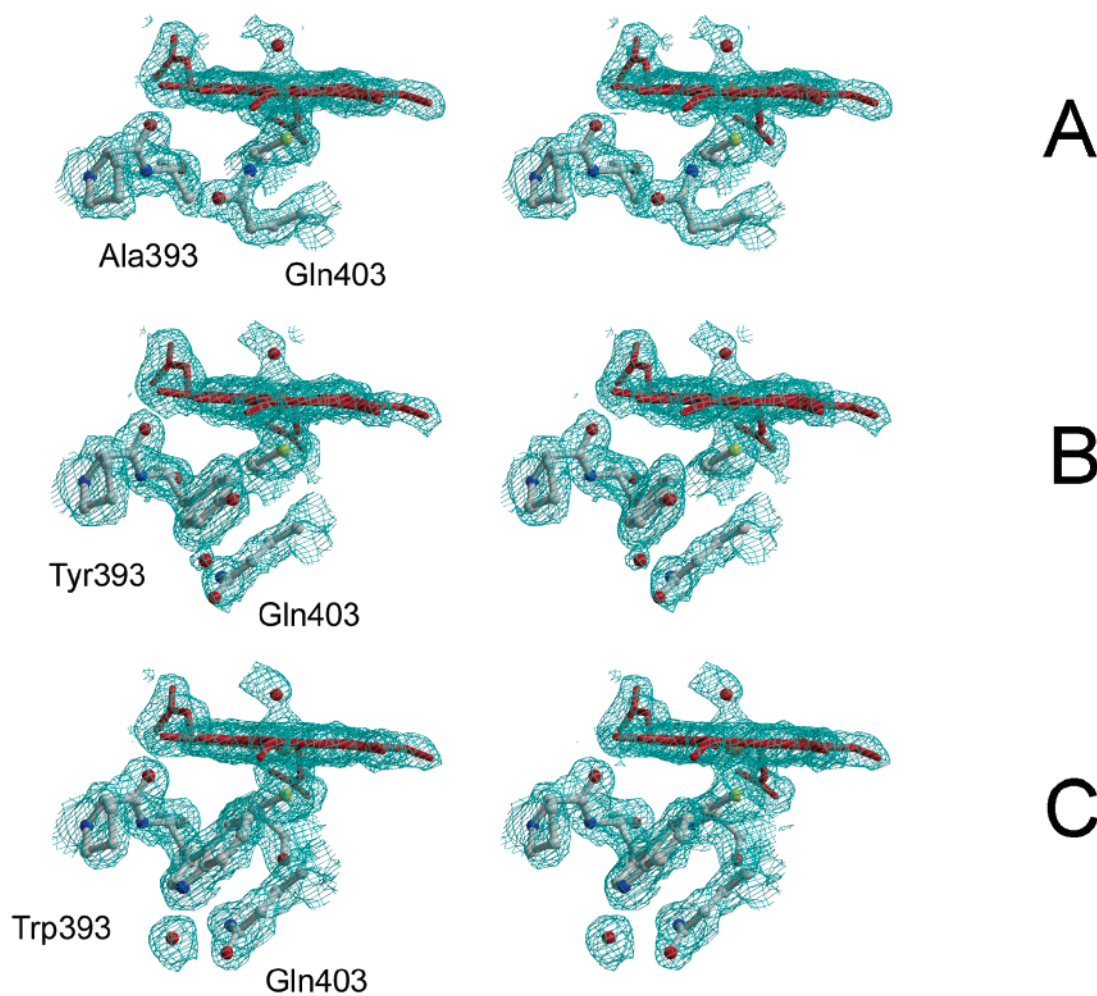

Figure 6. Stereoviews of the heme-binding region of P450 BM3 F393A (A), F393Y (B), and F393W (C). Electron density is shown in cyan, while the heme and peptide are shown in atom-type colors (red = O; blue = N; yellow = S; orange = Fe). In each case, the substituted residue (X393) and the important glutamine 403 (Gln403) are labeled. The electron density map was calculated using Fourier coefficients $(2F_o - F_c)$, where F_o and F_c are the observed and calculated structure factors, respectively. The contour level is 1.0σ, where σ is the RMS electron density. This diagram was generated using BOBSCRIPT[46] and RASTER 3D[47].
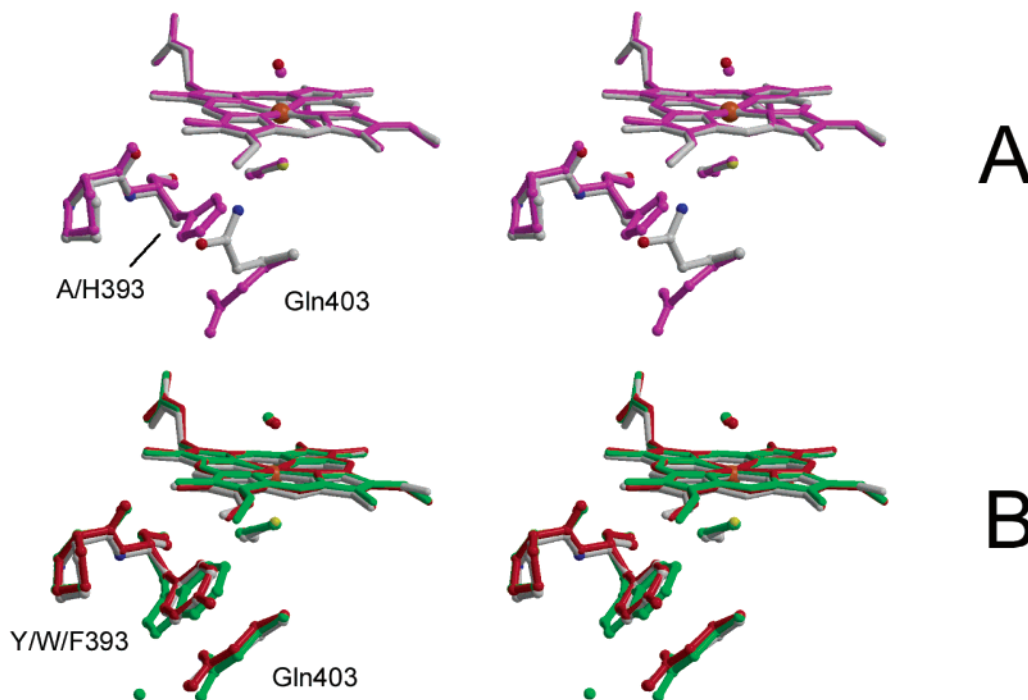
Figure 7. Overlaid stereoviews of the heme-binding region of P450 BM3 heme domain. Panel A shows the overlay of the F393A (atom type colors) and F393H (magenta) structures. Panel B shows the overlay of wild-type (atom type colors) with the F393Y (red) and the F393W (green) mutant structures. This diagram was generated using BOBSCRIPT[46] and RASTER 3D[47].

with the heme,[23] whereas the F393A mutant is unable to do this. The F393W-heme domain mutant structure (Figure 7b) shows that the indole nitrogen of Trp393 is not in the correct orientation to hydrogen-bond with Cys400, but the increased size of the residue side chain results in a closer interaction between it and the heme macrocycle. The F393W mutant has a more negative reduction potential than the wild-type enzyme. This is probably due to changes in the dielectric environment of the heme and its axial ligand, which appear to be heavily shielded from the aqueous solvent in this mutant enzyme.

Discussion

Substitutions of Phe393 of P450 BM3 have been shown to modulate the reduction potential of the heme over a 200 mV range, while retaining the structural integrity of the enzyme's active site. The fact that the active site of the enzyme is structurally unaffected by the mutations enables a quantitative examination of the effect of modulating heme reduction potential on individual steps in the P450 catalytic cycle. Consequently, we are able to probe the kinetics and thermodynamics of heme reduction and oxygen activation in a structurally consistent environment. The electronic properties of the flavins in the reductase domain of the enzyme have been shown to be unperturbed, both kinetically and thermodynamically, by the presence of the heme domain.[48] It is unlikely, therefore, that the mutations would have a significant influence on these cofactors.

P450 BM3 is a supremely efficient monooxygenase system, able to hydroxylate unactivated alkyl chains at rates of >100 s^{-1} (at 25 °C) with >95% coupling between substrates.[23,30] Coupling is aided by a mechanism, common in P450s, in which substrate binding induces a simultaneous spin-state shift (from

low to high-spin Fe^{III}) and a reduction potential increase to favor heme reduction. Consequently, the wild-type enzyme's turnover rate is 500-fold higher with substrate than without. The substrate-free F393A and -H mutants have similar reduction potentials to the substrate-bound wild-type enzyme; therefore, by comparing the heme reduction rates of the wild-type enzyme and the F393A or -H mutants (Table 1) and assuming that the mutations only affect the electronic properties of the heme, we are able to calculate the individual contributions of the spin-state shift and the reduction potential shift to the overall acceleration effect. These factors have been the subject of intense scrutiny,[16,31] but to date, the importance of the relative contribution of each effect remains experimentally unverified. Despite its similar reduction potential, the substrate-free F393A mutant has a 200-fold slower turnover rate than the substrate-bound wild-type enzyme. Conversely, the substrate-bound F393W mutant, which has a 70 mV lower reduction potential, is only 50% slower. It is clear, therefore, that the spin-state shift is the dominant activation mechanism and is 100-fold more important than the reduction potential shift. The rate constants for heme reduction add further insight; these are low for all the substrate-free enzymes, which have low-spin heme and increase by at least 70-fold on substrate binding. For the substrate-bound enzymes, the rate constants for heme reduction increase linearly with reduction potential (Figure 8) but only by a factor of 8 over 200 mV. Clearly this is not enough to cause a 500-fold increase in k_{cat} on substrate binding. The results are consistent with nonadiabatic electron transfer theory,[32] which predicts a Gaussian dependence of electron-transfer rate on driving force (ΔG). The linear relationship obtained is almost certainly an artifact of the limited reduction potential range studied; the plot would be expected

(30) Narhi, L. O.; Fulco, A. J. *J. Biol. Chem.* **1986**, *261*, 7160−7169.

(31) Honeychurch, M. J.; Hill, A. O.; Wong, L.-L. *FEBS Lett.* **1999**, *451*, 351− 353.

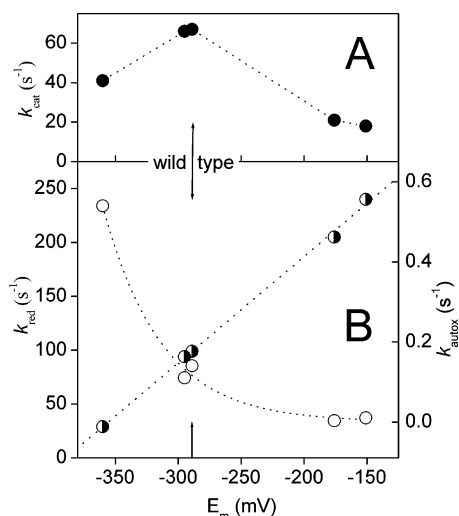(32) Marcus, R. A.; Sutin, N. *Biochem. Biophys. Acta* **1985**, *811*, 265−322.

Figure 8. Dependence of kinetic parameters on reduction potential. Panel A shows the plot of k_{cat} versus reduction potential (●); panel B shows the plot of k_{red} (left axis, ◑, fitted to a straight line) and k_{autox} (right axis, ○, fitted to an exponential decay) versus reduction potential. The arrow denotes the position of wild-type P450 BM3.

to adopt Gaussian characteristics out with this range. Certainly, it is difficult to believe that k_{et} would drop to zero at -375 mV as suggested by the ordinate intercept. Nevertheless, the clear trend observed with reduction potential does suggest that the electron-transfer rate is not being heavily perturbed by structural changes at the heme–flavin interface, which would be likely to introduce random scatter. The mutated residue does lie within the proposed area of interdomain contact[50] and may be involved in a pathway for electron transfer, but the structural changes induced by the mutations appear to have little effect on the rate of electron transfer; i.e., there is only an 8-fold variation across the series, which correlates with the shifts in the heme reduction potential.

Electron transfer in the substrate free enzyme is complicated by the fact that the heme is low-spin, six-coordinate ferric prior to reduction but becomes high-spin ferrous afterwards. The driving force for electron transfer in this case depends on the reduction potential of the heme in a fixed low-spin six-coordinate environment, which is likely to be very negative. Electron transfer may also be initiated by spontaneous spin-state equilibration. In this case, the proportion of heme in the high-spin state (populated thermally) determines the rate of electron transfer. Both mechanisms appear to be extremely inefficient for all the enzymes studied, until a large-scale spin-state shift is induced by substrate binding.

Various steps in the P450 catalytic cycle have been postulated to be rate determining. These include the following: transfer of the first electron to the heme (this is certainly the step activated by substrate binding); transfer of the second electron; oxygen activation (possibly involving protonation of a peroxo-ferric species); and product release.[1-4] It is also likely that the rate-determining step will vary between different P450 enzymes, given the variety of redox partners and substrates utilized by these systems. Nevertheless, all P450s share the same mechanism of oxygen activation. All the intermediate heme-oxy complexes on the catalytic pathway are unstable, making their characterization difficult. Great progress has recently been made in this area by Sligar, Petsko, and co-workers,[14] who have used time-dependent X-ray crystallography to obtain structures and

spectra of the oxy-ferrous and oxyferryl complexes of P450cam under cryogenic conditions.

Generation of the oxy-ferrous P450 complex[33] is the initial oxygen activation step, but this species is not directly involved in substrate hydroxylation.[34] In the absence of additional reducing equivalents, it decays spontaneously to ferric P450 and superoxide (autoxidation). While this is an unproductive reaction so far as catalysis is concerned, the rate of autoxidation is a quantitative measure of the stability of the oxy-ferrous species. As shown in Figure 8, the rate of decay increases exponentially as the reduction potential of the heme decreases for the mutants studied, which suggests a direct relationship between the heme reduction potential and the activation energy for dissociation of superoxide. This is clearly reasonable for a simple bond scission event. Scheme 1 illustrates the relationship between the heme reduction potential and the rate of autoxidation. The reduction potential of the dioxygen/superoxide couple is constant at approximately -160 mV; therefore, changes in the reduction potential of the heme will be manifested solely in changes to the equilibrium dissociation constants for dioxygen (K_{ox}) and superoxide (K_{sox}) from oxy-ferrous heme. The rate constants for association are second order and diffusion controlled and are therefore unlikely to show much dependence on reduction potential. The dissociation rate constant for dioxygen (k_{-ox}), on the other hand, is likely to be affected by changes in the Fe^{II}–dioxygen bond energy

The oxy-ferrous complex is shown in Scheme 1 along with its alternative resonance form, the superoxy-ferric complex; however, the true nature of the complex lies somewhere between these two extremes. The oxy-ferrous/superoxy-ferric content of this complex is determined by the relative positions of the Fe 3d-orbital energy levels and the oxygen π^* orbital after bonding. This will also determine the strength of bonding and, therefore, the rate of autoxidation. A simplified MO diagram is shown in Figure 9.[19] According to this model, the oxy-ferrous/superoxy-ferric character of the complex is determined by the energy gap (Δ) between the iron d_π (d_{xz}, d_{yz}) and the $\pi^*_{O_2}$ molecular orbitals. If Δ is large, the low-spin complex with oxy-ferrous character will be favored. Decreasing Δ results in the population of the $\pi^*_{O_2}$ orbital and superoxy-ferric character. In our series of mutants, Δ will be dependent on the energy of the Fe d_{xz},d_{yz} orbitals prior to oxygen binding, which will determine both their position relative to the $\pi^*_{O_2}$ orbital and the magnitude of their bonding interaction with it. The energy of the Fe d_{xz},d_{yz} orbitals relates directly to the reduction potential of the heme and is likely to be dependent on the π-donor strength of the thiolate axial ligand. Additional H-bonding interactions (i.e., in the F393A and F393H mutants) are likely to weaken the π-donor ability of the thiolate and increase the reduction potential of the heme. Electrostatic interactions between the imidizolium ion that may have been formed in the F393H mutant and the heme would also lower the energy of the Fe 3d-orbitals and increase the reduction potential of the heme. The π-bonding interaction between the d_{xz} and $\pi^*_{O_2}$ orbitals will shift electron density from the iron to the oxygen and will cause the two orbitals to move further apart in energy. However, if the π-bonding interaction is weak, then an increase in the energy of the d orbitals caused

(33) Peterson, J. A.; Ishimura, Y.; Griffen, B. W. *Arch. Biochem. Biophys.* **1972**, *149*, 197–208.
(34) Lipscomb, J. D.; Sligar, S. G.; Namtvedt, M. J.; Gunsalus, I. C. *J. Biol. Chem.* **1976**, *251*, 1116–1124.
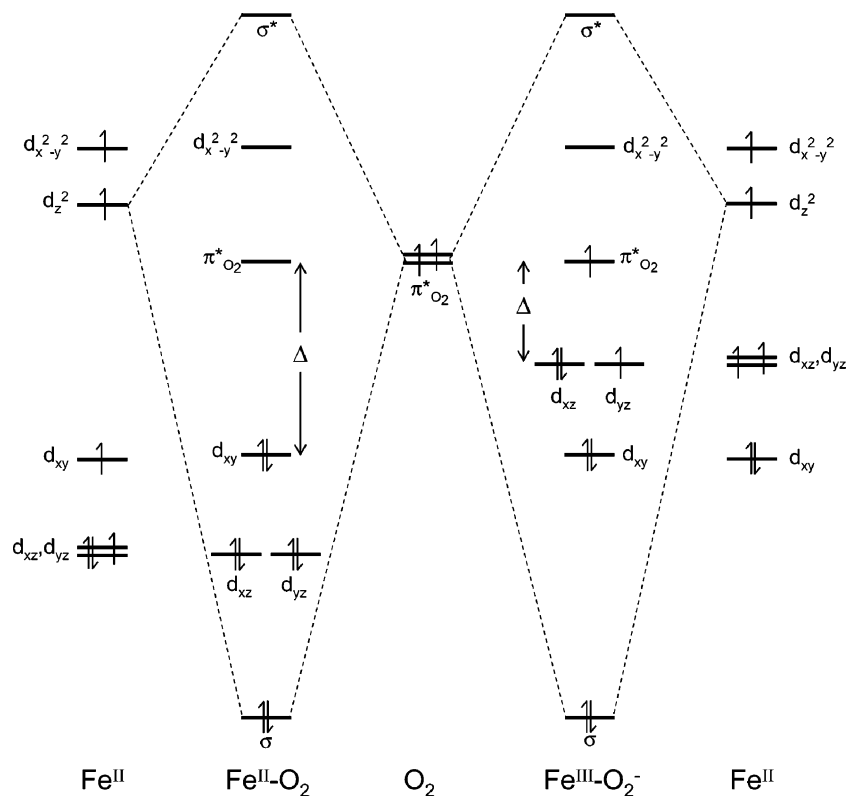
Figure 9. Qualitative molecular orbital diagram for P450 oxy-ferrous complexes (adapted from ref 19). This scheme illustrates how possible changes in the π-donor character of the axial ligand could cause changes in Δ. The two situations shown are where Δ > pairing energy ($Fe^{II}-O_2$) and where Δ < pairing energy ($Fe^{III}-O_2^-$).

by a mutation (e.g., F393W) will take the nonbonding d_{yz} orbital closer in energy to the $\pi^*_{O_2}$ orbital giving the electrons a greater tendency to unpair.

Some insight into the nature of the oxy-ferrous complex can be gained from the long-wavelength visible spectra shown in Figure 5. Panel A shows the spectra of high-spin ferric, low-spin ferric, and carbonmonoxy-ferrous forms of wild-type P450 BM3. Compared with these are the spectra of oxyhemoglobin (panel B) and the oxy-ferrous complexes of the F393A, WT, and F393W mutants of P450 BM3 (panel C). The bond vibrational energy of bound dioxygen in oxyhemoglobin determined using FTIR spectroscopy (v_{O-O} = 1107 cm^{-1}) indicates that the oxy-ferrous form of oxyhemoglobin has much of its electron density delocalized across the dioxygen bond.[35,36] Panel C compares the spectra of the oxy-ferrous complexes of the P450 BM3 enzymes. The spectrum of the F393A mutant closely resembles the carbonmonoxy-ferrous form of the enzyme, with fused α and β bands. That of the F393W mutant resembles the ferric low-spin spectrum and that of oxyhemo-globin, whereas the spectrum of the wild-type oxy-ferrous complex is intermediate. This trend is likely to be caused by changes in the energies of the Fe 3d orbitals in the oxy-ferrous complex and may reflect a shift in the balance of oxy-ferrous/superoxy-ferric character or a shift of electron density toward the oxygen, as a result of changes in the π-bonding properties of the heme axial ligand. It is impossible to determine the electronic configuration of the complex from the visible absorption spectra alone. However, the changes observed do

show that the oxyferrous complexes of the mutants are different and have altered electronic properties.

In our series of mutants the active-site structure is retained, making it unlikely that interactions between bound dioxygen and active site residues could have been altered. Other oxygen-binding hemoproteins utilize active-site residues to stabilize bound dioxygen. Both the globins and peroxidases form stabilized oxy-ferrous heme complexes in which histidine residues (and also an Arg for peroxidase) interact with the bound dioxygen.[37,38] The active sites of P450s are often hydrophobic, with proton delivery occurring via an active-site Thr residue (Thr268 in P450 BM3) working in tandem with an Asp.[39] This environment is likely to disfavor occupation of the oxygen π orbitals, either through a spin-state change or via bonding interactions. The overall result is an activated P450 oxy-ferrous complex in which its stability with respect to superoxide dissociation (which is decreased by a lower heme reduction potential) is balanced against its rate of reduction. Measuring the rate of electron transfer to the oxyferrous complex directly is beyond the scope of this study, but either this step or a protonation event leading to oxygen activation is a likely rate-determining step for the F393A and -H mutants. There is a complex relationship between k_{cat} and the heme reduction potential in the P450 BM3 mutants (Table 1). At low potentials, electron transfer to the heme is clearly rate determining, whereas, at high potentials, a subsequent catalytic step becomes important (Figure 8). The increased stability of the oxyferrous complexes observed is an indication that the second electron transfer event

(35) Momenteau, M.; Reed, C. A. *Chem. Rev.* **1994**, *94*, 659−698.
(36) Wittenberg, J. B.; Wittenberg, B. A.; Peisach, J.; Blumberg, W. E. *Proc. Natl. Acad. Sci. U.S.A.* **1970**, *67*, 1846−1853.

(37) Phillips, S. E.; Schoenborn, B. P. *Nature* **1981**, *292*, 81−82.
(38) Miller, M. A.; Shaw, A.; Kraut, J. *Nat. Struct. Biol.* **1994**, *1*, 524−531.
(39) Yeom, H.; Sligar, S. G.; Li, H.; Poulos, T. L.; Fulco, A. J. *Biochemistry* **1995**, *34*, 14733−14740.

may have been slowed. There are two mechanisms by which a second electron can be accepted by the heme system: (1) An electron can be transferred directly into the dioxygen π^* orbital. This orbital is, however, further from the electron donor (FMN) and is high in energy. (2) If the dioxygen π^* orbital is already populated to some extent, the electron can transfer into the Fe d_{yz} orbital, which will now be half-filled. This would be more favorable. Thus, the electronic nature of the oxyferrous complex holds the key to the subsequent steps of catalysis and warrants further investigation.

Recent studies on P450cam[39,40] and nitric oxide synthase[41] (NOS) have shown that removal of hydrogen bonds to the thiolate heme ligand decreases the reduction potential of the iron. Introducing such hydrogen bonds clearly has the opposite effect, as demonstrated in this study[23] and that of Ueyama et al.[42] It is likely that the presence/absence of a hydrogen bond affects the iron reduction potential by modulating the π- and σ-donor characteristics of the thiolate ligand. It is also interesting to compare the oxy-ferrous complexes of P450cam and P450 BM3. The visible spectrum of the former has fused α and β bands, and the complex is relatively stable ($k_{autox} = 0.001$ s^{-1}). These properties are remarkably like those of the F393A and F393H mutants of P450 BM3 and may indicate that their 3d orbitals are of similar energy. It is also worth noting that the camphor-bound reduction potential of P450cam is also similar to those of the mutants (-175 mV). In P450cam, electron transfer is rate limiting, primarily due to the requirement for formation of the productive P450/putidaredoxin complex.[43,44]

For P450cam, a stable oxy-ferrous complex may be required to compensate for any delay in the delivery of the second electron from putidaredoxin. For P450 BM3, the integral reductase domain ensures the rapid delivery of two successive electron equivalents[49] and the stability of the oxy-ferrous complex is poised to maximize the rates of both.

In summary, we have shown that decreases in the heme reduction potential lead to heme reduction being rate limiting, whereas increases in the heme reduction potential lead to increases in the stability of the oxy-ferrous complex. The latter may result in the second FMN to heme electron transfer being rate limiting. The 3d orbital energies of the heme-iron in wild-type P450 BM3 are optimized such that both the first electron transfer and the subsequent oxygen activation steps occur at similar rates, maximizing the overall rate of catalytic turnover. We have also shown that the first electron transfer is gated almost entirely by the substrate-induced spin-state shift and that the contribution of the simultaneous reduction potential shift is negligible by comparison.

(40) Yoshioka, S.; Takahashi, S.; Ishimori, K.; Morishima, I. *J. Inorg. Biochem.* **2000**, *81*, 141−151.
(41) Adak, S.; Crooks, C.; Wang, Q.; Crane, B. R.; Tainer, J. A.; Getzoff, E. D.; Stuehr, D. J. *J. Biol. Chem.* **1999**, *274*, 26907−26911.
(42) Ueyama, N.; Nishikawa, N.; Yamada, Y.; Okamura, T.; Oka, S.; Sakurai, H.; Nakamura, A. *Inorg. Chem.* **1998**, *37*, 2415−2421.
(43) Hui Bon Hoa, G.; Begard, E.; Debye, P.; Gunsalus, I. C. *Biochemistry* **1978**, *17*, 2835−2839.
(44) Hintz, M. J.; Mock, D. M.; Peterson, L. L.; Tuttle, K.; Peterson, J. A. *J. Biol. Chem.* **1982**, *257*, 14324−14332.

(45) Nahri, L. O.; Fulco, A. J. *J. Biol. Chem.* **1987**, *262*, 6683−6690.
(46) Esnouf, R. M. *J. Mol. Graphics* **1997**, *15*, 132−136.
(47) Merritt, E. A.; Bacon, D. J. *Methods Enzymol.* **1997**, *277*, 505−524.
(48) Daff, S. N.; Chapman, S. K.; Turner, K. L.; Holt, R. A.; Govindaraj, S.; Poulos, T. L.; Munro, A. W. *Biochemistry* **1997**, *36*, 13816−13823.
(49) Sevrioukova, I.; Shaffer, C.; Ballou, D. P.; Peterson, J. A. *Biochemistry* **1996**, *35*, 7058−7068.
(50) Sevrioukova, I. F.; Li, H. Y.; Zhang, H.; Peterson, J. A.; Poulos, T. L. *Proc. Natl. Acad. Sci.* **1999**, *96*, 1863−1868.